Weak Lensing Mass Reconstruction of the Galaxy Cluster Abell 209

S. Paulin-Henriksson, V. Antonuccio-Delogu
INAF / Osservatorio Astrofisico di Catania, Via Santa Sofia 78, I-95123 Catania, Italy

We describe step by step the typical weak gravitational lensing analysis of the galaxy cluster Abell 209 ($z \sim 0.2$), using a heavily modified version of the KSB algorithm applied to an archival R-band image of this cluster taken with the CFHT-12k. A parametric modelling with NFW profile gives a total mass within R_{200} of about $2 \times 10^{15}\ M_{\odot}$, slightly larger than the value derived by Mercurio et al.[10] using radial velocities.

1 Introduction

The galaxy cluster Abell 209 ($z = 0.209$) is a particularly interesting target for a weak lensing mass reconstruction, because it is probably not completely virialised[4,10,3], is well covered by observations and the evolutionary properties of its galaxy populations have already been meticulously analysed[4,10].

This contribution describes the analysis perfomed on a deep R-band image, based on the KSB+ weak lensing analysing method[7,8,6], throught a pipeline implemented at the Catania Astrophysical Observatory (Italy) and tested on STEP simulated images [5,9]. This work is a preliminary step towards a more complete forthcoming analysis in R and B bands.

2 Data description

We use archival CFHT-12k images in R band, reduced and stacked by Haines, Mercurio et al.[4,10] in the framework of their photo-spectrometric analysis. These data were kindly provided by the Capodimonte observatory (Italy). Data are complete for $R \lesssim 25$.

As this analysis is perfomed directly on stacked images, the overlaps between CCD may contain some PSF (Point Spread Function) instabilities. For this reason we mask these overlapped regions. Unfortunately, the cluster center lies exactly within such a CCD overlap. We extend the data with a HST/WFPC2 field of about 1 arcmin in the broad red filter F702W, centered on the cluster center.

3 The weak lensing analysis

3.1 Step 1 - building star and background galaxy catalogues

The weak lensing signal is carried by background galaxies, lensed by the foreground cluster. On the other hand, stars carry the information about the PSF. The first step of the analysis is to build star and background galaxy catalogues.

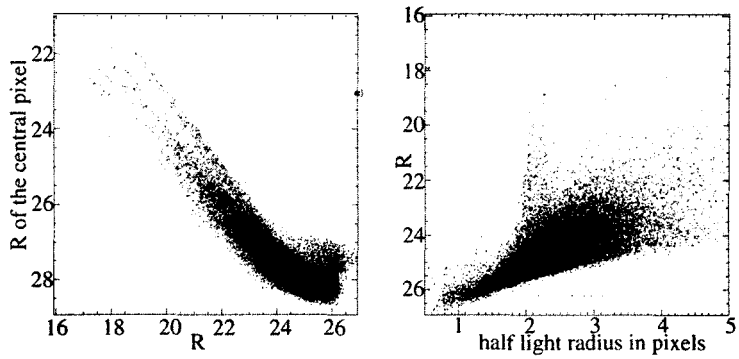

Figure 1: Left panel: magnitude - central magnitude diagram for all objects detected in the R-band image. Right panel: radius - magnitude diagram for the same objects. In both panels, stars are in red. Cluster (background respectively) galaxies are in light (dark resp.) blue. Other objects (black and dark purple) are excluded from the analysis.

The star identification is made in the 3 parameter space r_h, R, $R_{\max}$. r_h is the half-light-radius (eg. the radius inside which one have 50% of the total flux of the object), R is the magnitude in the R band, and $R_{\max}$ is the magnitude of the central pixel (eg. the pixel containing the centroid estimated by SExtractor[2]). Figure 1 shows the star sequence in red. It is important to note that all these 3 parameters are necerssary for the star selection. Typically 10% of the objects that would be selected as stars by 2 of the 3 parameters, are finally rejected by the third parameter. Finally we get an average star density of $\sim 0.22.\text{arcmin}^{-2}$ (eg. ~ 22 stars per CCD).

The foreground / background galaxy selection is a straightforward cut on R. The values for this cut are choosen to give an almost uniform background galaxy density (while the foreground galaxy density is highly peaked around the cluster center), and will be optimised in future. After the mask, the averaged background galaxy density all over the field is $\sim 15.\text{arcmin}^{-2}$. This number will be optimised when we will include the B image in the analysis.

3.2 Step 2 - PSF interpolation

The PSF is interpolated from stars, independently for each CCD, using a 2-degree-2-dimentional polynomial for each of 6 components of the PSF properties, as required by the KSB method. This is illustrated with the ellipticity on figure 2. The fact that, after the smearing and anisotropy corrections, the PSF shows such small and smooth variations all around the field, even from a CCD to another, is not at all assumed at any step of the analysis. It is a sign of the very good data quality.

3.3 Step 3 - Tests of the PSF subtraction

To test the PSF subtraction, we perform three statistical tests:

1. We study the correlations between corrected galaxy ellipticities and uncorrected star ellipticities, as shown on figure 3 (a, b, c, d): As expected, the significant correlation due to the PSF before any correction is not significant anymore after the PSF subtraction.

2. We study the correlations between the intensity of the shear $|\gamma|$ and object size for different magnitude bins, as shown on figure 3 (e). As expected for most of the rg bins, the error bars do not overlap and one clearly see that the weak lensing signal increases with the

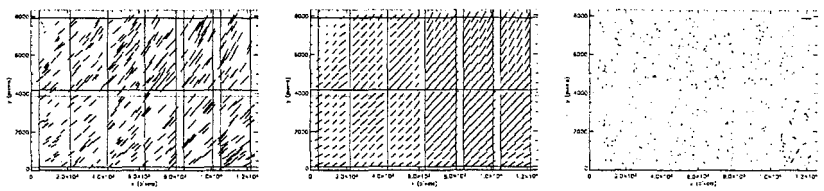

Figure 2: Star ellipticities over the field (for a window radius of 2 pixels, see the KSB analysing method details). Left panel: before corrections (i.e. observed ellipticities). Middle panel: PSF interpolated from the left panel. Right panel: residuals of the fit. In all panels, vectors lie along the major axis, while their length is proportional to the ellipticity: $|\epsilon| = \frac{\sqrt{(Q_{11}-Q_{22})^2+4Q_{12}^2}}{Q_{11}+Q_{22}}$. The scale shown in the upper right corners is $|\epsilon| = 0.05$. The straight lines show the CCD overlaps, which are not taken into account in the interpolation process.

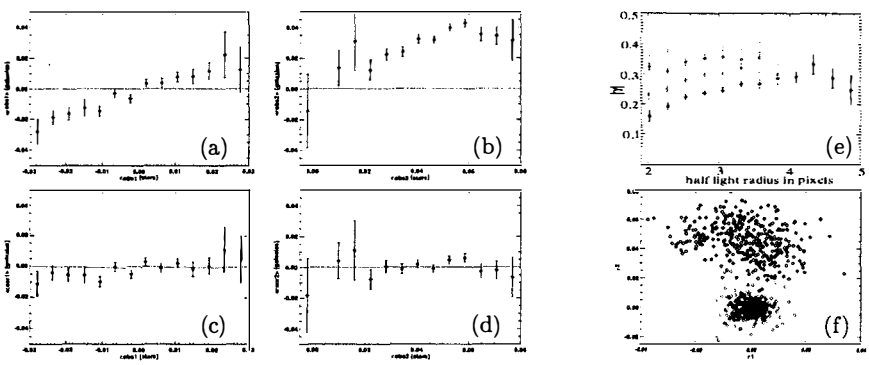

Figure 3: Panels a and c (b and d respectively): $< \epsilon_1 >_{\rm bin}$ ($< \epsilon_2 >_{\rm bin}$ resp.) of galaxies with respect to ϵ_1 (ϵ_2 resp.) of the nearest star. Panels a and b (c and d respectively) show the significant (unsignificant resp.) correlation before (after resp.) the anisotropic correction. Panel e: Average value $< |\gamma| >_{\rm bin} = < \sqrt{\gamma_1^2+\gamma_2^2} >_{\rm bin}$ of galaxies as a function of $r_{1/2\,\Phi}$, for 4 different magnitude bins. In black: $17.5 \lesssim R \lesssim 20.0$ (i.e. the 25% brightest galaxies), in red: $20.0 \lesssim R \lesssim 20.8$, in dark blue: $20.8 \lesssim R \lesssim 21.4$, and in light blue: $21.4 \lesssim R \lesssim 25.8$ (i.e. the 25% faintest galaxies). Panel f: ϵ_1 against ϵ_2 of stars before (black) and after (red) the anisotropic correction.

magnitude, ultimately with the optical depth. Note that the error bars do include the errors on the measured ellipticity.

3. We compare star corrected and uncorrected ellipticities, as shown on figure 3 (f). As expected after the subtraction, the distribution is centered around 0, with a very lower standard deviation.

3.4 Step 4 - Mass reconstruction

Fitting a NFW profile

We have used parametric mass reconstruction to get a preliminary estimate of the mass within a given aperture. We fit a NFW (Navarro-Frenk-White)[11] to the tangential shear data[14]. The maximum likelihood values for the two NFW free parameters are: $r_{200} = 2.0\,h^{-1}\,$Mpc and $M_{200} = 1.9 \times 10^{15}\,M_\odot$. r_{200} is the radius inside which the average density is equal to 200 times the cosmological critical density, and M_{200} is the mass inside r_{200}.

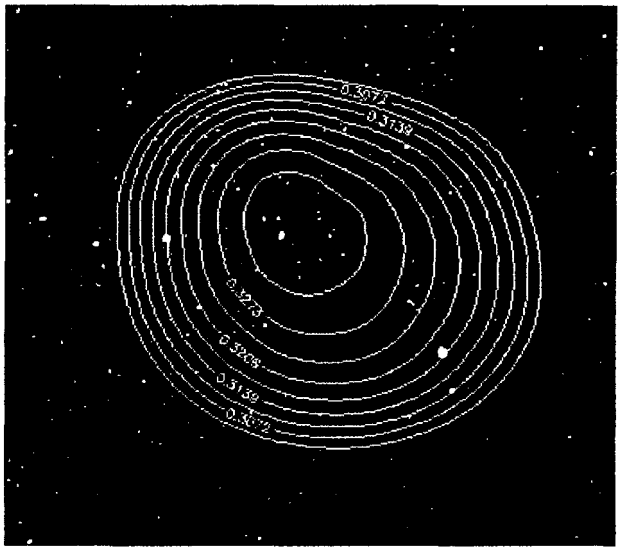

Figure 4: Mass reconstructed profile. The box is about $10' \times 10'$ wide (1 pixel = $0.206''$), which, at the redshift of A209 ($z = 0.209$) corresponds to about 2.5 h^{-1} Mpc. Contours are logarithmically spaced and the central contour corresponds to a surface mass density of $0.25 \times 10^5\ M_{\odot}.\mathrm{arcmin}^{-2}$

Direct mass reconstruction

We have used the method described in Seitz & Schneider[13], based on the solution of a Poisson equation for the quantity $K = \ln(1-\kappa)$, where: $\kappa = \sigma/\Sigma_{crit}$ is the projected surface density in units of the critical density[1]. The resulting profile is shown in figure 4. The elongation of the isodensity contour hints at the presence of two clumps of galaxies which have recently merged, as suggested by previous analysis[10].

Acknowledgments

This work is supported by the European Commission, VI Framework Program for Reserach and Development, *Marie Curie* Project MTKD-CT-2004-002995 "COSMOCT" .

References

1. Bartelmann M., King, L.J. and Schneider P., 2001, A&A, 378, 361
2. Bertin E. and Arnouts S., 1995, A&A, 117, 393
3. Giovannini G. Feretti L., Govoni F. et al., astro-ph/0601285
4. Haines C.P., Mercurio A., Merluzzi P. et al., 2004, A&A, 425, 783
5. Heymans C., Van Waerbeke L., Bacon D. et al., 2006, MNRAS, 368, 1323
6. Hoekstra H., Franx M., Kuijken K. et al., 1998, ApJ, 504, 636
7. Kaiser N., Squires G. and Broadhurst T., 1995, ApJ, 449, 460
8. Luppino G.A. and Kaiser N., 1997, ApJ, 475, 20
9. Massey R., Heymans C., Bergé J. et al., 2006, under development
10. Mercurio A., Busarello, G., Merluzzi, P. et al., 2004, A&A, 424, 79
11. Navarro J.F., Frenk C.S, and White S.D.M., 1997, ApJ, 490, 493
12. Paulin-Henriksson S. , Antonuccio-Delogu V. et al., under development
13. Seitz S. and Schneider, P., 2001, A&A, 374, 740
14. Wright C.O. and Brainerd T.G., 2000, ApJ, 534, 34